The Influence of Wind Forcing on the Chesapeake Bay Buoyant Coastal Current*

STEVEN J. LENTZ

Woods Hole Oceanographic Institution, Woods Hole, Massachusetts

JOHN LARGIER

Bodega Marine Laboratory, University of California, Davis, Davis, California

ABSTRACT

Observations of the buoyant coastal current that flows southward from Chesapeake Bay are used to describe how the thickness, width, and propagation speed vary in response to changes in the along-shelf wind stress. Three basic regimes were observed depending on the strength of the wind. For weak wind stresses (from −0.02 to 0.02 Pa), the buoyant coastal current was relatively thin, the front slope was not steep, and the width was variable (1–20 km). For moderate downwelling (southward) wind stresses (0.02–0.07 Pa), wind-driven cross-shelf advection steepened the front, causing the plume to narrow and thicken. For stronger downwelling wind stresses (greater than 0.07 Pa), vertical mixing dominated, bulk Richardson numbers were approximately 0.25, isopycnals were nearly vertical, and the plume front widened but the plume width did not change. Plume thickness and width were normalized by the theoretical plume scales in the absence of wind forcing. Normalized plume thickness increased linearly from 1 to 2 as downwelling wind stresses increased from 0 to 0.2 Pa. Normalized plume widths were approximately 1 for downwelling wind stresses from 0.02 to 0.2 Pa. The observed along-shelf propagation speed of the plume was roughly equal to the sum of the theoretical propagation speed and the wind-driven along-shelf flow.

1. Introduction

Observations and numerical model studies have shown that wind forcing has a profound influence on the characteristics of buoyant coastal currents from rivers or estuaries because the wind-driven momentum flux is trapped in the relatively thin buoyant plume by the large density gradients separating the plume from the ambient fluid (e.g., Chao 1988; Blanton et al. 1989; Munchow and Garvine 1993; Kourafalou et al. 1996; Fong et al. 1997; Fong 1998; Hickey et al. 1998; Xing and Davies 1999; Rennie et al. 1999; Sanders and Garvine 2001; Berdeal et al. 2002). The following qualitative picture emerges from these studies. Upwelling-favorable along-shelf winds oppose the along-shelf propagation of buoyant coastal currents and can inhibit their formation. When a buoyant coastal current already exists at the onset of upwelling winds, the wind-driven offshore Ekman transport causes the plume to thin, widen, and eventually separate from the coast and move offshore (Fig. 1a) (Fong et al. 1997; Hallock and Marmorino 2002; Lentz 2004). For downwelling winds, the onshore Ekman transport causes the plume front to steepen and the plume to thicken, narrow, and flow more rapidly along shelf (Fig. 1b) (Rennie et al. 1999; Johnson et al. 2001). If the wind forcing is strong enough, rapid vertical mixing may result in vertical isopycnals and a wider plume front (Fig. 1c) (Blanton et al. 1989).

Recent studies have proposed simple models quantifying the response to upwelling winds as the buoyant plume separates from the coast and spreads offshore (Fong and Geyer 2001; Lentz 2004). Whitney and Garvine (2005) have recently proposed a wind strength index—the ratio of a characteristic plume speed to a characteristic wind-driven velocity—as a measure of whether the flow is wind or buoyancy driven. Whitney and Garvine also proposed a time scale for the initial iso-

Corresponding author address: Steven J. Lentz, Woods Hole Oceanographic Institution, MS 21, Woods Hole, MA 02543.
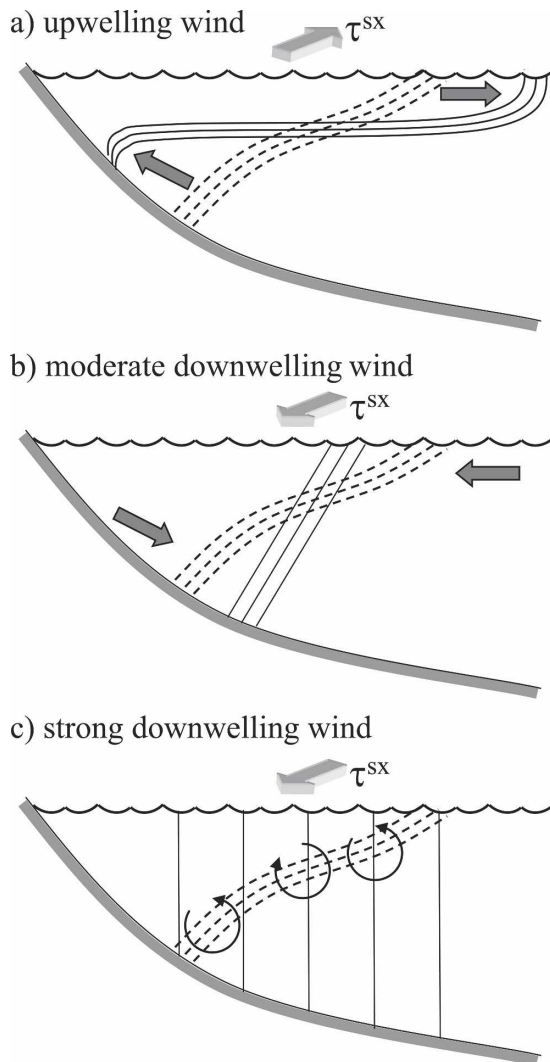E-mail: slentz@whoi.edu

FIG. 1. Schematic of buoyant plume response to different along-shelf wind forcing: (a) upwelling winds flatten the plume front, causing the plume to thin and widen; (b) moderate downwelling winds steepen the front, causing the plume to thicken and narrow; (c) strong downwelling winds force vertical mixing that widens the plume front, but causes little change in the plume width.

FIG. 2. Schematic of buoyant plume defining basic parameters. The water depth is $h(y)$, h_p is the maximum plume thickness where the plume front intersects the bottom a distance W_b offshore. The plume cross-sectional area onshore of W_b is A_b and offshore of W_b is A_s. The offshore distance from where the plume front intersects the bottom to where it intersects the surface is W_s.

pycnal slope dependence on wind stress that is proportional to the plume cross-sectional area divided by the Ekman transport (see also Fong and Geyer 2001; Lentz 2004). However, a general model that provides quantitative estimates of the dependence of buoyant coastal current characteristics, such as width, thickness, and propagation speed, on wind stress does not exist.

As an initial step toward quantifying the relationship between buoyant coastal current characteristics and wind forcing, the wind-driven response of the buoyant coastal current that flows southward from Chesapeake Bay is examined using observations obtained in 1994. Rennie et al. (1999) previously used the same observa-
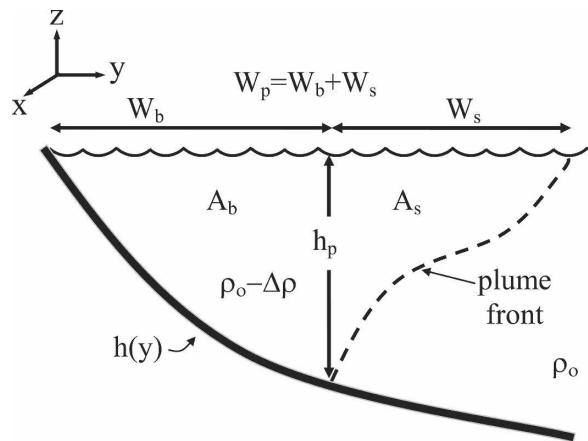
tions to describe the Chesapeake plume. There have been a number of studies characterizing the buoyant coastal current from Chesapeake Bay and its response to wind forcing (Boicourt 1973; Rennie et al. 1999; Johnson et al. 2001; Hallock and Marmorino 2002; Lentz et al. 2003; Lentz 2004). This study builds on the descriptions of Rennie et al. (1999) and Johnson et al. (2001) by determining the dependence on along-shelf wind stress of the plume thickness, width, and propagation speed in the context of a recent theory for buoyant coastal currents flowing along a sloping bottom in the absence of wind forcing (Lentz and Helfrich 2002). The objective is to provide a general framework that can be tested on other buoyant coastal currents. The focus is on downwelling-favorable wind stresses because even moderate upwelling-favorable wind stresses cause the Chesapeake plume to separate from the coast, at which point it may no longer propagate along shelf as a buoyant coastal current (Rennie et al. 1999; Hallock and Marmorino 2002; Lentz 2004).

2. Background

a. Scaling theory

Lentz and Helfrich (2002) propose a simple theory for buoyant coastal currents in the absence of wind forcing that provides estimates of the geometry, flow, and propagation speed given the density anomaly of the plume $\Delta\rho$, the plume transport Q, the Coriolis parameter f (latitude), and the bottom slope α. Their estimates are based on a constant bottom slope. As out-

lined below, it is straightforward to extend their derivation to a more general bathymetry that varies in the cross-shelf direction, $h(y)$ (Fig. 2), and therefore can be more readily applied to observations.

Following Yankovsky and Chapman (1997), assume that the along-plume flow is geostrophic, concentrated at the plume front, and zero at the bottom under the front (so there is no bottom stress). The depth where the front separating the buoyant coastal current from the ambient shelf water intersects the bottom (h_p) is

$$h_p \approx \left(\frac{2Qf}{g'} \right)^{1/2},$$ (1)

where $g' = g\Delta\rho/\rho_o$ is reduced gravity, g is the gravitational acceleration, and ρ_o is a reference density (Chapman and Lentz 1994; Yankovsky and Chapman 1997; Lentz and Helfrich 2002). This estimate of the plume thickness does not depend on the characteristics of the bathymetry.

The offshore distance from the coast to where the front intersects the bottom (W_b) can be determined from the bathymetry; that is, W_b is the y location where $h(y = W_b) = h_p$. The distance from the foot of the front to the offshore edge of the plume (W_s) is assumed to scale with the baroclinic deformation radius based on h_p (Hsueh and Cushman-Roisin 1983),

$$W_s \approx \frac{c_w}{f},$$ (2)

where $c_w = \sqrt{g'h_p}$ is the internal wave speed. The total plume width at the surface is $W_p = W_b + W_s$.

The propagation speed of the nose of the buoyant coastal current (c_p) is estimated by noting that volume conservation implies that $Q\Delta t = A_p c_p \Delta t$ if the nose shape does not vary and entrainment is small. Here A_p is the cross-sectional area of the plume and Δt is a time increment. Solving for the propagation speed

$$c_p = \frac{Q}{A_p} = \frac{c_w}{(1 + A_b/A_s)},$$ (3)

where $A_p = A_b + A_s$, and the plume cross-sectional areas onshore and offshore of the foot of the front are A_b and A_s, respectively (Fig. 2). The right-hand expression in (3) follows from (1), (2), and assuming a triangular geometry so that $A_s \approx W_s h_p/2$; A_b is determined by integrating $h(y)$ from $y = 0$ (the coast) to $y = W_b$.

The key nondimensional parameter in this case is A_b/A_s. [This reduces to the nondimensional parameter c_w/c_α, discussed by Lentz and Helfrich (2002), if the bottom slope is constant, where $c_\alpha = \alpha g'/f$.] If A_b/A_s is

small, the buoyant coastal current is "surface trapped," $c_p \approx c_w$, and $W_p \approx W_s$, consistent with buoyant gravity currents propagating along a wall (e.g., Griffiths 1986). If A_b/A_s is large, the buoyant coastal current is "slope controlled," $c_p \approx c_\alpha \equiv Q/A_b$, and $W_p \approx W_b$ (Chapman and Lentz 1994; Yankovsky and Chapman 1997).

In the presence of wind forcing, the propagation speed of the plume can be estimated as $c_{wnd} = Q/A_p$, assuming there is not substantial entrainment of ambient shelf water so that the cross-sectional area of the buoyant coastal current is conserved. In this case the total transport is $Q = Q_{wnd} + Q_g$, where $Q_{wnd} = u_w A_p$ is the wind-driven along-shelf transport and $Q_g = g'h_p^2/(2f)$ is the geostrophic transport associated with the thermal wind balance in the plume front (as for the case of no wind). The wind-driven flow u_w is estimated by assuming that the bottom stress balances the wind stress using a linear drag law with a drag coefficient r to represent the bottom stress, so $u_w = \tau^{sx}/(\rho_o r)$. Substituting these expressions into the expression for c_{wnd} yields

$$c_{wnd} = \frac{\tau^{sx}}{\rho_o r} + c_p,$$ (4)

where c_p is given by (3). Thus, the propagation speed is still c_p relative to the wind-driven ambient flow, but the total propagation speed is the sum of the ambient flow and the propagation speed, as previously noted for inviscid gravity currents along a wall (Simpson 1982). Note, however, that the wind forcing may alter c_p by changing the plume geometry and the density anomaly through wind-driven entrainment. Normalizing by c_p yields

$$\frac{c_{wnd}}{c_p} = 1 + \frac{\tau^{sx}}{\rho_o r c_p}.$$ (5)

The term $\tau^{sx}/\rho_o r c_p$ in (5) is similar to the wind strength index proposed by Whitney and Garvine (2005). Equations (4) or (5) provide an estimate of the buoyant plume propagation speed in terms of τ^{sx}, Q, r, g', $h(y)$, and f. These estimates of the propagation speed dependence on wind stress may not be appropriate for the case of strong wind forcing when there may be significant entrainment of ambient shelf water (Fig. 1c) that could change the momentum of the plume.

b. Measurements

The characteristics of the Chesapeake Bay buoyant coastal current are determined from moored and shipboard measurements obtained from August through
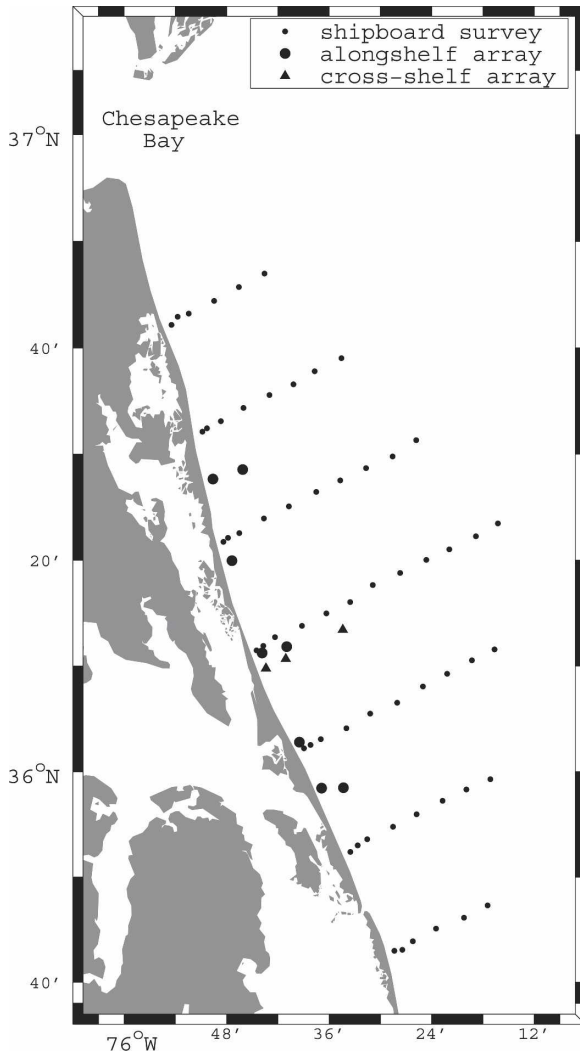
FIG. 3. Map of the study region, located south of Chesapeake Bay, showing the moored instrument locations and the station locations for the large-scale hydrographic surveys.

FIG. 4. Cross-shelf salinity section obtained from a small-boat survey (▼ indicate station locations) during a buoyant coastal current event on 31 Aug 1994. The vertical and cross-shelf location of instruments on the cross-shelf moored array are also shown. Salinity color scale is on the right.

October 1994 in a region extending from 35 to 150 km southeast of Chesapeake Bay (Fig. 3). A cross-shelf array of moorings was deployed about 90 km south of the mouth of Chesapeake Bay. This central line included moorings in water depths of 4 m, 8 m, 13.5 m, 21 m, and 26 m with current and temperature sensors spanning the water column (Fig. 4). Temperature–conductivity sensors were also deployed at 4- and 7-m depths on the Field Research Facility (FRF) pier near the 8-m site; at 1.5-, 7.7-, and 12.2-m depths at the 13.5-m site; at 2.1-, 7.6-, 14.2-, and 19.7-m depths at the 21-m site; and at 2.1-, 7.6-, 14.2-, and 24.7-m depths at the 26-m site. Temperature–conductivity instruments were deployed about 0.5 m above the bottom at five sites spaced about 15 km apart along the 5-m
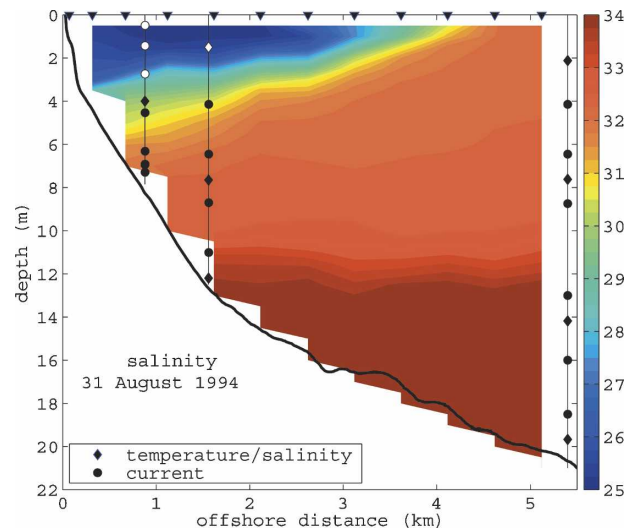
isobath. Observations from this along-shelf array are used to estimate the along-shelf propagation speed of the buoyant plume (Rennie et al. 1999). The sample rate for the moored instruments was typically 4 min.

Continual shipboard hydrographic surveys were conducted during the months of August and October. These included large-scale surveys (shown in Fig. 3), small-scale surveys consisting of five cross-shelf transects extending 20 km offshore, and additional cross-shelf transects along the central line. Along-shelf separations between cross-shelf transects were about 20 km for the large-scale surveys and 10 km for the small-scale surveys. Station spacing on cross-shelf transects was 2–5 km. The large-scale surveys took about 2 days to complete and the small-scale surveys took about 1 day. Thus, these surveys do not provide synoptic maps of the buoyant coastal current events, which typically lasted a few days and evolved substantially over times scales of hours. Daily cross-shelf transects extending 5 km offshore at the central line and taking 2 h to complete were also made using a small boat from August through October (Fig. 4). The station spacing of these sections was about 0.5 km. Observations from the ship and small-boat surveys are used to estimate the buoyant coastal current width and thickness during varying wind stress conditions. The small-boat surveys were limited to periods of weak winds, while the ship surveys included periods of moderate, but not strong, wind stresses (Fig. 5b).
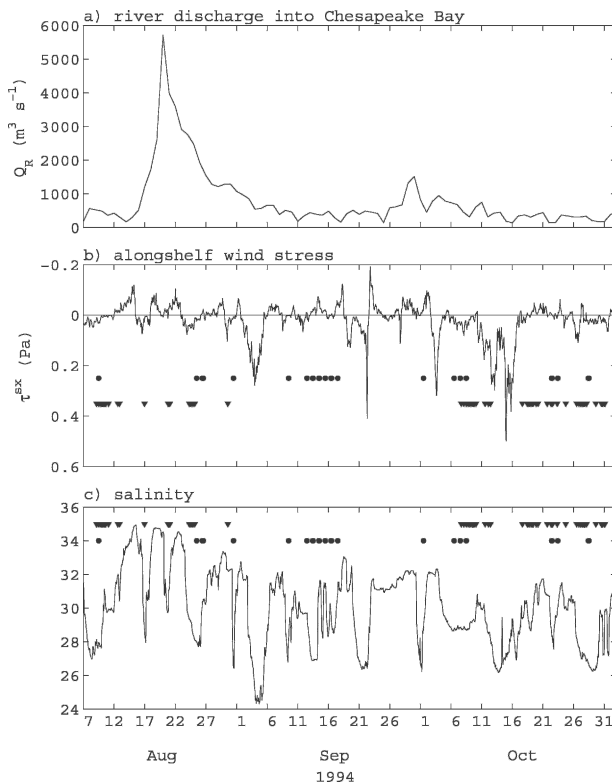
FIG. 5. Time series of (a) the river discharge into Chesapeake Bay, (b) the along-shelf wind stress at the FRF pier, with positive (downwelling) stress directed toward the south along shelf, and (c) the salinity at 4-m depth on the FRF pier. Wind stress axis has been inverted to facilitate comparisons with salinity time series. Times of ship (▼) and small boat (●) surveys are also shown in (b) and (c). Note that small boat surveys only occurred during weak winds, while ship surveys included moderate winds.

c. Estimation of terms

Wind stress is estimated, following Large and Pond (1981), using wind measurements from the end of the FRF pier. Correlation scales for the wind in this region are about 600 km (Austin and Lentz 1999), indicating that the FRF wind stresses are representative of the entire Chesapeake Bay buoyant coastal current. Accurate estimates of the buoyant current transport Q are not available because the moored observations do not resolve the entire plume. Consequently, the average net transport out of Chesapeake Bay, $Q = 10\,200$ m^3 s^{-1}, estimated from the time-averaged salt budget (Austin 2002), is used here. This estimate neglects temporal variations in Q associated, for example, with the wind (Valle-Levinson et al. 2001), and assumes that all of the transport from Chesapeake Bay goes into the buoyant coastal current. For comparison, sea level observations in Chesapeake Bay were used to estimate the net barotropic transport out of the bay during plume release

events (Rennie et al. 1999). This estimate of Q does not account for baroclinic exchange. Both estimates of Q yield similar results (see section 3a), therefore $Q = 10\,200$ m^3 s^{-1} is used as an estimate of the average buoyant current transport during plume events.

The observed plume thickness, h_{obs}, is estimated as the depth at which the plume front intersects the bottom in each CTD section. This estimate is uncertain because of both the coarse station spacing, particularly in the ship surveys, and the uncertainty in choosing one location for a finite-width plume front (see, e.g., Fig. 4). Given h_{obs} and the bathymetry $h(y)$, the offshore distance to the foot of the front W_{bobs} can be determined. The cross-shelf bathymetry, $h(y)$, is from bathymetric surveys along the central line (see Fig. 4 and 9). The width of the plume at the surface, W_{obs}, is determined from the underway salinity measurements on the ship because it provides better spatial resolution than the CTD stations. For the small-boat surveys, W_{obs} is determined from the CTD sections. To determine the plume scales h_p and W_p, reduced gravity g' is estimated using the observed density difference between the offshore ambient water and the minimum density within the plume for each hydrographic section, with $g = 9.8$ m s^{-2}, $\rho_o = 1020$ kg m^{-3}, and the Coriolis parameter $f = 8.58 \times 10^{-5}$ s^{-1}.

To test (4) or (5), observations from the array of five temperature–conductivity sensors deployed along the 5-m isobath were used. The observed propagation speed c_{obs} was estimated as the separation between adjacent along-shelf sites divided by the difference in the arrival time of the nose of the plume at the two sites. To determine the propagation speed scale, c_p given by (3), g' was estimated from the density jump as the nose of the plume passed each site. The plume thickness h_p was estimated from (1) using the estimates of g' and Q. Given h_p, W_s is estimated from (2) and W_b is estimated from the bathymetry $h(y)$. Finally, the cross-sectional plume areas A_s and A_b were determined from W_s, W_b, and $h(y)$. To estimate the wind-driven flow u_w for each estimate of c_{obs}, the average of τ^{sx} over the time interval between the arrival of the nose at the two sites is used with $r = 5 \times 10^{-4}$ m s^{-1} (Lentz et al. 1999). Observations from Johnson et al. (2001) taken in the same region during the spring of 1997 are included in the analysis using reported wind stresses and propagation speeds from Table 1 of their paper and estimating density jumps from Fig. 1 of their paper.

3. Results

Freshwater transports into Chesapeake Bay from August through October 1994 were about 500 m^3 s^{-1},
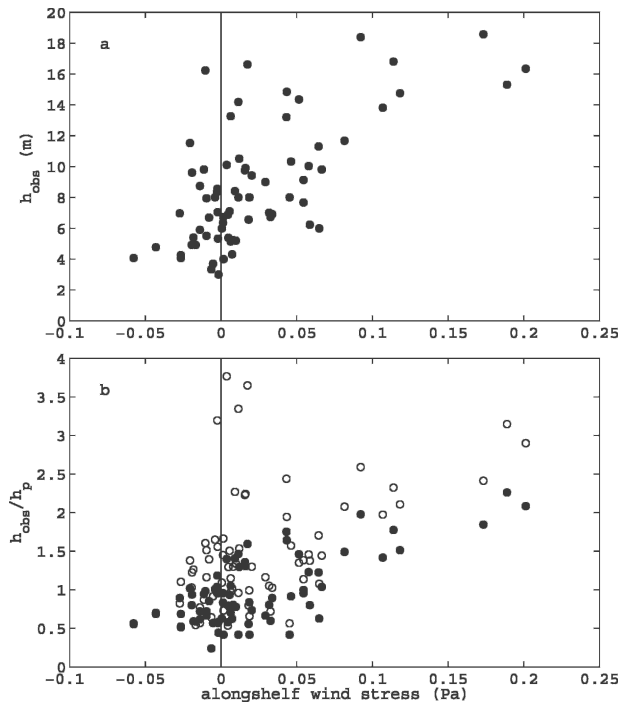
FIG. 6. Observations from ship surveys of buoyant gravity current (a) thickness h_{obs} and (b) normalized thickness h_{obs}/h_p as a function of the along-shelf wind stress. Estimates of h_p in (b) are based on a constant Q (filled symbols) and a variable Q (open symbols) estimated from sea level data within Chesapeake Bay.

FIG. 7. Observations from ship surveys of buoyant gravity current (a) width W_{obs} and (b) normalized width W_{obs}/W_p as a function of along-shelf wind stress. Estimates of W_p in (b) based on a constant Q (filled symbols) and a variable Q (open symbols) estimated from sea level data within Chesapeake Bay.

except for an event in mid-August when freshwater transport exceeded 5000 m³ s⁻¹ (Fig. 5a). During most of the study period wind stresses fluctuated between ±0.1 Pa (Fig. 5b). However, there were five down-welling events when wind stresses exceeded 0.2 Pa. Buoyant plumes intermittently propagated southeast-ward along the coast and were evident at the mooring sites as pulses of low-salinity (<30 psu) water lasting a day to a week (Fig. 5c). The buoyant coastal current events are related to wind forcing at the mouth of the bay, which periodically dams up and then releases the buoyant estuarine water (Rennie et al. 1999; Valle-Levinson et al. 2001). Consequently, the buoyant coastal current events are often preceded by down-welling-favorable wind stresses and do not exhibit an obvious relationship to the freshwater transport into Chesapeake Bay. A total of 15 events were identified for which there was clear evidence of an along-shelf-propagating buoyant coastal current.

a. Plume geometry

The ratio A_b/A_s estimated from the ship salinity sections ranges from 0.15 to 0.35 during weak winds for the Chesapeake buoyant coastal current events in August–
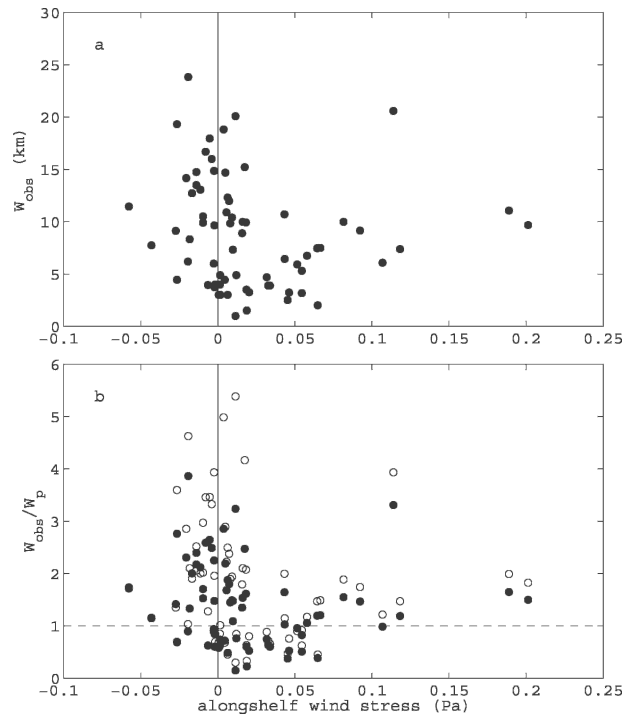
October 1994, indicating a more surface-trapped buoyant coastal current, as opposed to a slope-controlled buoyant coastal current. Thus, the scaling theory of Lentz and Helfrich (2002) predicts that in the absence of wind forcing $c_p \approx c_w = \sqrt{g'h_p}$ and $W_p \approx c_w/f$ for the Chesapeake buoyant coastal current.

As noted previously by Rennie et al. (1999), the Chesapeake buoyant coastal current is thinner and wider during upwelling-favorable winds ($\tau^{sx} < 0$) and thicker and narrower during downwelling-favorable winds ($\tau^{sx} > 0$: Figs. 6a and 7a). The plume front also steepens for increasing (downwelling) winds (Fig. 8). Plume thicknesses h_{obs} are 3–10 m for small wind stresses, increasing to about 15 m for downwelling wind stresses of 0.1–0.2 Pa (Fig. 6a). The observed thicknesses normalized by h_p from (1) range from 0.5 to 1.5 for weak wind stresses, increasing at a roughly linear rate to 2.5 for $\tau^{sx} = 0.2$ Pa (Fig. 6b). For weak or upwelling-favorable wind stresses ($\tau^{sx} < 0.02$ Pa), observed buoyant coastal current widths (W_{obs}) vary from 1 to 25 km and do not exhibit a clear dependence on wind stress (Fig. 7a). For $\tau^{sx} > 0.02$ Pa, W_{obs} tends to increase from a few kilometers to about 10 km for $\tau^{sx} = 0.2$ Pa. The observed widths normalized by W_p also
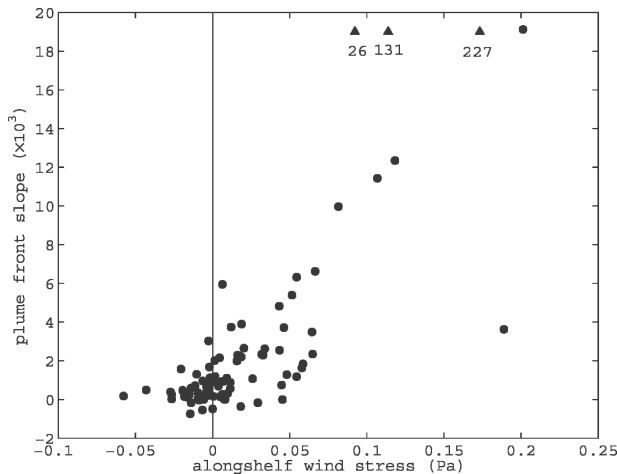
FIG. 8. Observed slope of the plume front as a function of along-shelf wind stress. The magnitude ($\times 10^{-3}$) of three very steep slopes that are offscale ($\blacktriangledown$) are noted near the top of the figure.
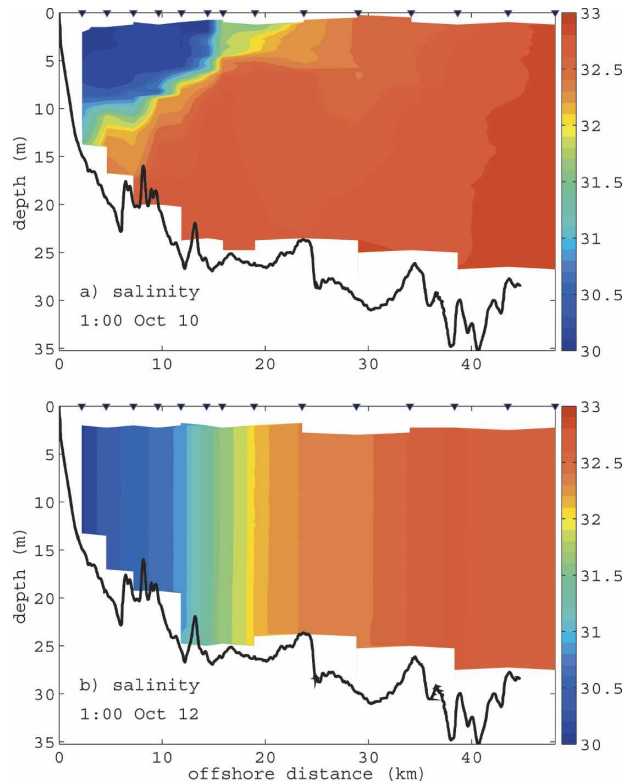

FIG. 9. Cross-shelf salinity sections on (a) 10 Oct, when winds were weak, and (b) 12 Oct, after the onset of strong downwelling winds (see Fig. 10). Station locations are indicated ($\blacktriangledown$) at the top of each section and the salinity color scale is shown to the right.

exhibit large scatter for weak wind stress magnitudes, with normalized widths ranging from 0.5 to 4. For moderate wind stresses (0.02–0.07 Pa), normalized widths tend to be less than 1. For the few wind stress events in excess of 0.07 Pa, normalized widths tend to be 1–2, with one notable exception discussed below. The constant and variable Q estimates yield similar results for the dependence of the normalized thickness and width on along-shelf wind stress. The variable Q estimates for the study period tend to be less than the constant value of 10 200 $\mathrm{m^3\,s^{-1}}$, resulting in slightly larger normalized thicknesses and widths.

Wind forcing influences buoyant coastal currents both through advection and mixing (Fig. 1). Thinner plumes during weak or upwelling winds are particularly sensitive to the wind stress because the wind-driven momentum is trapped in a thinner layer (Lentz 2004). This may explain the large variations in W_{obs} during weak winds. For moderate downwelling wind stresses the tendency for W_{obs}/W_p to be less than 1 (Fig. 7b) is consistent with the wind-driven cross-shelf circulation moving the plume front onshore at the surface and offshore at the bottom and, hence, steepening the front (Fig. 1b). However, for stronger downwelling wind stresses the observations indicate that vertical mixing dominates over cross-shelf advection. Figure 9 shows two salinity sections—the first just prior to the onset of strong downwelling wind stresses ($\tau^{sx} > 0.2$ Pa) and the second two days later after sustained downwelling wind stresses (Fig. 10a). Both the salinity sections (Fig. 9) and the salinity time series from the 13-, 21-, and 26-m moorings (Figs. 10b–d) indicate that the water column is rapidly homogenized after the onset of downwelling

wind stresses, except possibly close to the bottom at the 26-m site. The tendency for the near-surface salinities to increase and the deeper salinities to decrease without a substantial change in the depth-averaged salinity suggests that the homogenization is due to vertical mixing rather than advection. The 12 October plume event corresponds to the anomalously wide plume event during strong downwelling wind stresses ($\tau^{sx} \approx 0.1$ Pa) in Fig. 7b. This plume is wide because it was wide prior to the onset of the wind forcing (Fig. 10a), possibly because of weak upwelling winds that preceded the downwelling wind event.

Previous analyses indicate that in this shallow water, the wind-driven cross-shelf circulation is essentially shutdown when the water column becomes well mixed during strong wind stresses (Lentz 2001). This is consistent with $W_{obs}/W_p \approx 1$ during strong downwelling wind stresses (Fig. 7b) because vertical mixing shuts down the cross-shelf circulation before there is a change in the plume width. The result is that the total plume width at the surface does not change, but the width of the plume front increases (cf. Figs. 9a and 9b).
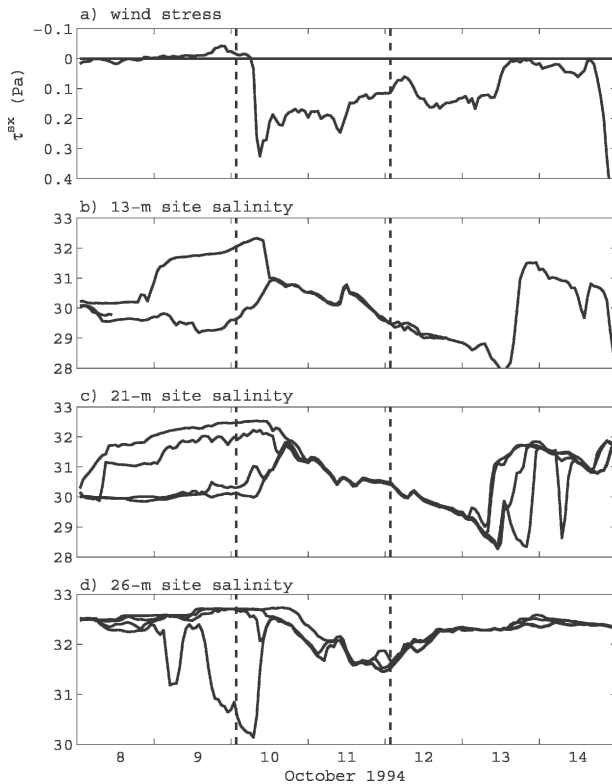
FIG. 10. Time series of the (a) along-shelf wind stress, (b) salinity at 1.5- and 12.2-m depths at the 13.5-m site, (c) salinity at 2.1-, 7.6-, 14.2-, and 19.7-m depths at the 21-m site, and (d) salinity at 2.1-, 7.6-, 14.2-, and 24.7-m depths at the 26-m site for 8–14 Oct 1994. The vertical dashed lines indicate the times of the salinity sections shown in Fig. 9.
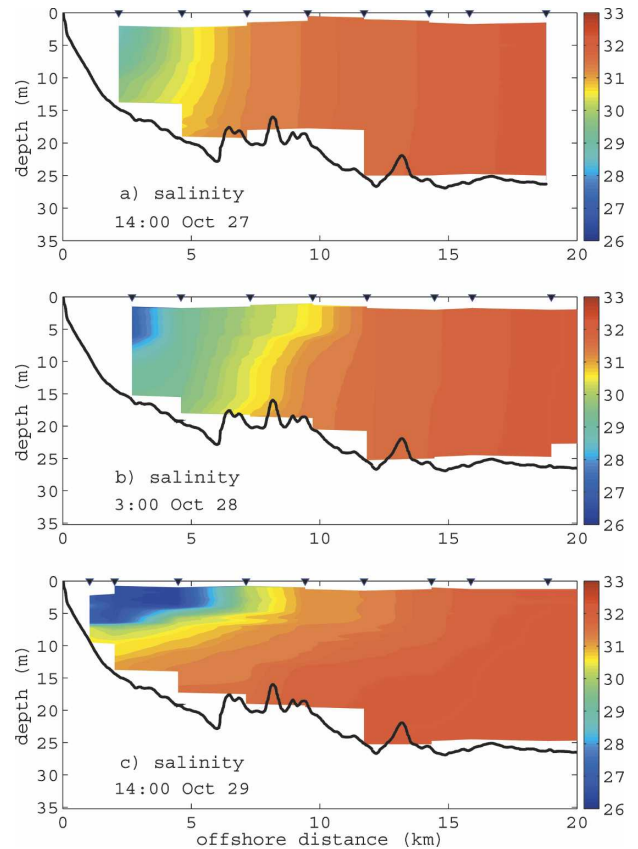

FIG. 11. Cross-shelf salinity sections taken (a) 27 Oct during strong winds, (b) 28 Oct, and (c) 29 Oct, as winds decreased (see Fig. 12). Station locations are indicated (▼) at the top of each section and the salinity color scale is shown to the right.

After a strong downwelling wind stress event, the nearly vertical isopycnals relax, moving offshore near the surface and onshore near the bottom (Figs. 11 and 12). However, the broader plume front remains.

To further investigate the vertical mixing during wind-forced plume events, estimates of the bulk Richardson number

$$\mathrm{Ri}_B = \frac{g\Delta\rho h}{\rho_o(\Delta u)^2}$$

at the 13-m site were calculated using hourly differences between the moored near-surface and near-bottom density and velocity to estimate $\Delta\rho$ and Δu, respectively. To focus on plume events, only times when the near-surface salinities were less than 29 psu are considered (see Fig. 5). For $\tau^{sx} < 0.07$ Pa, Ri_B is typically greater than 1 (Fig. 13a). For $\tau^{sx} > 0.07$ Pa (downwelling), Ri_B is less than 1 and fluctuates around 0.25 (dashed line). Sanders and Garvine (2001) found a similar relationship between Ri and wind stress near the mouth of Delaware Bay. The associated vertical

shear is oriented along shelf and tends to be in thermal wind balance with the cross-shelf density gradient. The along-shelf shear $\partial u/\partial z$ increases as τ^{sx} increases for $\tau^{sx} < 0.07$ Pa, but then is relatively constant for $\tau^{sx} > 0.07$ Pa (Fig. 13b), corresponding to a mixed water column (e.g., Fig. 9b). There is the suggestion that the shear may decrease for larger wind stresses, but there are only a few data points at the larger wind stresses.

b. Propagation speed

Observed propagation speeds ranged from 0.25 to 1 m s^{-1} (Fig. 14). Theoretical propagation speeds in the absence of wind forcing ranged from 0.2 to 0.6 m s^{-1} and were not significantly correlated with c_{obs} (Table 1 and Fig. 14a). However, c_p and c_{obs} are correlated during weak wind stresses ($|\tau^{sx}| < 0.02$ Pa, Table 1 and solid symbols in Fig. 14a), with a regression coefficient of 1.5. Estimates of the wind-driven along-shelf flow in the absence of a buoyant coastal current, $u_w = \tau^{sx}/(\rho_o r)$, range from −0.02 to 0.9 m s^{-1}, and are weakly corre-
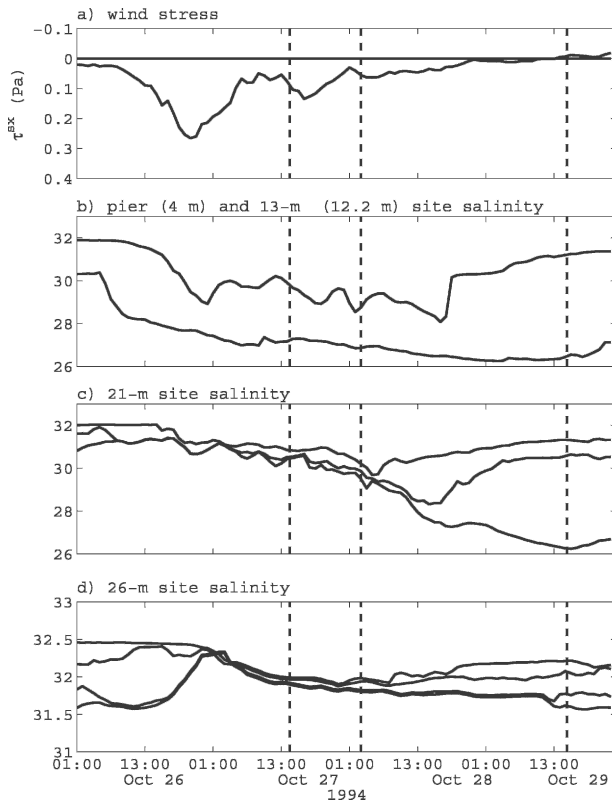
FIG. 12. Time series of (a) the along-shelf wind stress, (b) salinity at 4-m depth on the FRF pier and 12.2-m depth at the 13.5-m site, (c) salinity at 2.1-, 7.6-, and 14.2-m depths at the 21-m site, and (d) salinity at 2.1-, 7.6-, 14.2-, and 24.7-m depths at the 26-m site for 26–29 Oct 1994. The vertical dashed lines indicate the times of the salinity sections shown in Fig. 11.

FIG. 13. Estimates from the 13-m site of (a) the bulk Richardson number Ri_B and (b) the vertical shear in the along-shelf velocity $\Delta u/\Delta z$ as a function of the along-shelf wind stress during buoyant coastal current events (near-surface salinity less than 29 psu). Estimates of Ri_b and $\Delta u/\Delta z$ are obtained from hourly differences between near-surface and near-bottom currents and densities. The horizontal dashed line in (a) represents $Ri_B = 0.25$.

lated with c_{obs} (Table 1 and Fig. 14b). The correlation between the combined estimate c_{wnd} from (4) and c_{obs} is larger than the correlation between either u_w or c_p and c_{obs} (Fig. 14c). The regression coefficient is 0.6 and the intercept is 0.2 m s^{-1} (Table 1). The nondimensional form of the observed propagation speed (5) shows that, for near-zero wind forcing, c_{obs}/c_p ranges between 0.8 and 1.6 and that there are relatively few events when the wind forcing has a substantial impact on the propagation speed; that is, $\tau^{sx}/(\rho_o r c_p)$ is rarely greater than 1 (Fig. 15).

4. Discussion

One obvious limitation of this analysis is the estimates of the buoyant coastal current transport used to determine h_p, W_p, and c_p. The transport out of Chesapeake Bay is a function of the wind stress and, hence, variable (Valle-Levinson et al. 2001). It also, almost certainly, depends on the baroclinic exchange. Further-
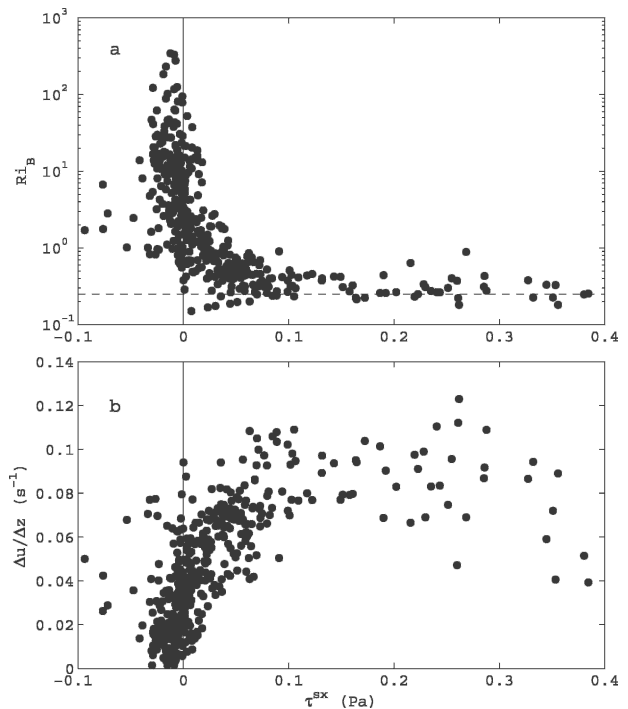
more, the relationship between the transport out of the bay and the buoyant coastal current transport is uncertain because of the possible accumulation of buoyant water near the mouth of Chesapeake Bay (Pichevin and Nof 1997). The relatively clear picture that emerges from this analysis reflects the weak dependence of the scale estimates on Q (Lentz and Helfrich 2002): from scaling theory (section 2a), one can see that h_p depends on $Q^{1/2}$, W_s and c_w depend on $Q^{1/4}$, and c_p depends on $Q^{1/4}$ for a surface-trapped plume or is independent of Q for a slope-controlled plume. Thus, the results do not imply that Q is relatively constant. Direct observations of the buoyant coastal current transport and its dependence on the wind forcing and freshwater transport into Chesapeake Bay are needed to address this issue further.

Along-shelf wind stresses may influence the nose propagation speed in three ways. First, larger downwelling wind stresses increase the ambient shelf flow and hence increase the propagation speed relative to land, even if the propagation speed relative to the ambient fluid remains unchanged. This result is consistent with early inviscid theory and the effect of a "head-
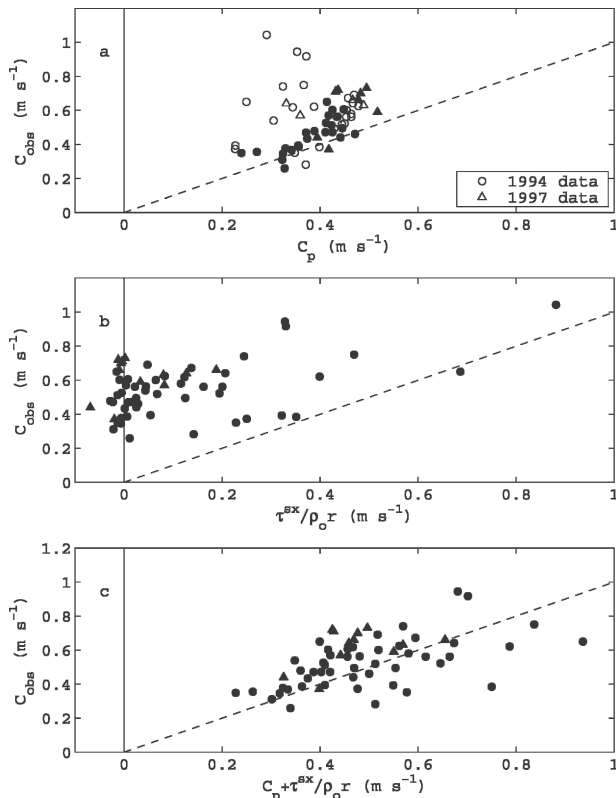
FIG. 14. Observed propagation speed c_{obs} vs (a) c_p, (b) $\tau^{sx}/(\rho_o r)$, and (c) $c_p + \tau^{sx}/(\rho_o r)$. Dashed lines have a slope of 1.0. Solid symbols in (a) highlight estimates for which $|\tau^{sx}| < 0.02$ Pa. The 1997 observations (triangles) are from Johnson et al. (2001).
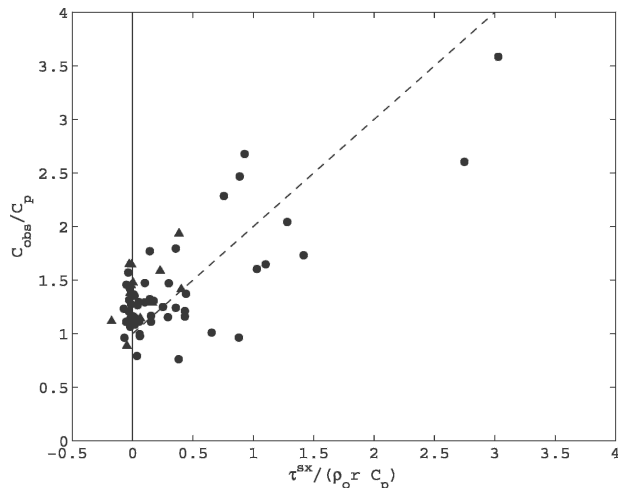

FIG. 15. Normalized observed propagation speed c_{obs}/c_p as a function of normalized wind forcing $\tau^{sx}/(\rho_o r c_p)$. Dashed line has a slope of 1.0 and a y intercept of 1.0.

wind" on nonrotating buoyancy flows (e.g., Simpson 1982). Second, larger downwelling winds increase the plume thickness (Fig. 6a), increasing c_p and hence increasing the propagation speed. Third, larger downwelling wind stresses tend to correspond to smaller density anomalies, presumably due to more vertical mixing. This results in a reduced g' and a smaller c_p and hence decreases the propagation speed. Estimates of c_p based on observations of g' and h_p from ship or small boat surveys do not exhibit any obvious dependence on wind stress. This suggests that there is a tendency for the

dependencies on g' and h_p to compensate. In other words, there is a counterbalance between effects two and three listed above, and the primary effect of wind forcing is to change the flow in the ambient fluid and thereby influence the plume propagation as an inviscid effect. The generality of this result is unclear.

The observations during weak winds provide some of the first observational support for the relevance of the scalings proposed by Lentz and Helfrich (2002) to the ocean (though see Lentz et al. 2003). For weak wind stresses the normalized plume thicknesses (h_{obs}/h_p) are 0.5–1.5 for a constant Q (Fig. 6). Normalized plume widths exhibit a wide range from 0.5 to 4 during weak wind stresses (Fig. 7), presumably because the width of relatively small buoyant coastal currents, such as the Chesapeake plume, are sensitive to even weak up-welling wind events (Lentz 2004). This suggests that the width scale W_p may not provide accurate width estimates for moderate to small buoyant coastal currents subject to even weak, variable winds. However, the tendency for the normalized plume width to be about one for moderate to strong downwelling winds provides some support for the proposed width scale and underscores the role of downwelling winds in "organizing" the plume by constraining the plume width and inhibiting dispersal. For weak wind stresses the normalized propagation speeds (c_{obs}/c_p) range from 0.8 to 1.6 in support of the scale estimate (Figs. 15 and 14a). The average value of c_{obs}/c_p is 1.2 ± 0.1 for the Chesapeake buoyant coastal current in the absence of wind forcing, determined from the intercept of a linear regression of c_{obs}/c_p on $\tau^{sx}/(\rho_o r c_p)$. This result is in remarkable agreement with the scaling coefficients of 1.1, found by Stern

TABLE 1. Results of linear regression analyses of the form $c_{obs} = ax + b$, where x is either c_p, u_w, or c_{wnd}. There are 62 observations in each analysis, except there are 31 observations (c_p with asterisk) of c_p when $|\tau^{sx}| < 0.02$.

Variable	Slope	Intercept	Correlation
c_p	0.6 ± 0.6	0.3 ± 0.2	0.27
c_p^*	1.5 ± 0.5	-0.1 ± 0.2	0.76
u_w	0.4 ± 0.2	0.5 ± 0.04	0.47
c_{wnd}	0.6 ± 0.2	0.2 ± 0.1	0.62

et al. (1982), and 1.3, Griffiths and Hopfinger (1983), in laboratory studies of buoyant gravity currents propagating along a vertical wall. This is consistent with the observation that the influence of the bottom slope is weak for the Chesapeake buoyant coastal current ($A_b/A_s \approx 0.25$).

5. Summary

Observations of the buoyant coastal current from Chesapeake Bay indicate that the response to wind forcing is similar to the schematic shown in Fig. 1. For weak winds the buoyant coastal current thickness is roughly equal to the theoretical thickness scale h_p and the plume width is often large and variable, presumably because small buoyant coastal currents are sensitive to wind forcing, particularly upwelling winds (Lentz 2004). During downwelling-favorable winds the plume front steepens, the plume thickens, and the plume width is roughly equal to the theoretical plume width W_p. During moderate downwelling-favorable winds these changes appear to be primarily due to cross-shelf advection (as in Fig. 1b), and there is the suggestion that the plume width is actually slightly less than W_p. However, for stronger downwelling-favorable wind stresses (Fig. 1c), vertical mixing dominates, estimates of the bulk Richardson number are approximately 0.25, isopycnals are nearly vertical, the plume front widens, and the plume width does not change (e.g., Fig. 9).

When the wind stress is weak, the plume propagates at roughly the theoretical propagation speed c_p. During downwelling-favorable wind stresses the plume propagates at roughly the sum of c_p and the wind-driven ambient shelf flow ($\tau^{sx}/\rho_o r$, where τ^{sx} is the along-shelf wind stress and r is a linear drag coefficient). The Chesapeake buoyant coastal current is one example of a surface-trapped plume. Observations of other buoyant coastal currents are needed to determine the generality of these results both to other surface-trapped plumes and to slope-controlled plumes.

REFERENCES

Austin, J. A., 2002: Estimating the mean ocean–bay exchange rate of the Chesapeake Bay. *J. Geophys. Res.,* **107,** 3192, doi:10.1029/2001JC001246.

——, and S. J. Lentz, 1999: The relationship between synoptic weather systems and meteorological forcing on the North Carolina inner shelf. *J. Geophys. Res.,* **104,** 18 159–18 186.

Berdeal, I. G., B. M. Hickey, and M. Kawase, 2002: Influence of wind stress and ambient flow on a high discharge river plume. *J. Geophys. Res.,* **107,** 3130, doi:10.1029/2001JC000932.

Blanton, J. O., L.-Y. Oey, J. Amft, and T. N. Lee, 1989: Advection of momentum and buoyancy in a coastal frontal zone. *J. Phys. Oceanogr.,* **19,** 98–115.

Boicourt, W. C., 1973: The circulation of water on the continental shelf from Chesapeake Bay to Cape Hatteras. Ph.D. thesis, The Johns Hopkins University, 183 pp.

Chao, S. Y., 1988: Wind-driven motion of estuarine plumes. *J. Phys. Oceanogr.,* **18,** 1144–1166.

Chapman, D. C., and S. J. Lentz, 1994: Trapping of a coastal density front by the bottom boundary layer. *J. Phys. Oceanogr.,* **24,** 1464–1479.

Fong, D. A., 1998: Dynamics of freshwater plumes: Observations and numerical modeling of the wind-forced response and alongshore freshwater transport. Ph.D. thesis, MIT/WHOI Joint Program in Oceanography, 155 pp.

——, and W. R. Geyer, 2001: Response of a river plume during an upwelling favorable wind event. *J. Geophys. Res.,* **106,** 1067–1084.

——, ——, and R. P. Signell, 1997: The wind-forced response of a buoyant coastal current: Observations of the western Gulf of Maine plume. *J. Mar. Syst.,* **12,** 69–81.

Griffiths, R. W., 1986: Gravity currents in rotating systems. *Annu. Rev. Fluid Mech.,* **18,** 59–89.

——, and E. J. Hopfinger, 1983: Gravity currents moving along a lateral boundary in a rotating frame. *J. Fluid Mech.,* **134,** 357–399.

Hallock, Z. R., and G. O. Marmorino, 2002: Observations of the response of a buoyant estuarine plume to upwelling favorable winds. *J. Geophys. Res.,* **107,** 3066, doi:10.1029/2000JC000698.

Hickey, B. M., L. J. Pietrafesa, D. A. Jay, and W. C. Boicourt, 1998: The Columbia River plume study: Subtidal variability in the velocity and salinity fields. *J. Geophys. Res.,* **103,** 10 339–10 368.

Hsueh, Y., and B. Cushman-Roisin, 1983: On the formation of surface to bottom fronts over steep topography. *J. Geophys. Res.,* **88,** 743–750.

Johnson, D. R., A. Weidemann, R. Arnone, and C. O. Davis, 2001: Chesapeake Bay outflow plume and coastal upwelling events: Physical and optical properties. *J. Geophys. Res.,* **106,** 11 613–11 622.

Kourafalou, V. H., L.-Y. Oey, J. D. Wang, and T. N. Lee, 1996: The fate of river discharge on the continental shelf. 1. Modeling the river plume and the inner shelf coastal current. *J. Geophys. Res.,* **101,** 3415–3434.

Large, W. G., and S. Pond, 1981: Open ocean momentum flux measurements in moderate to strong winds. *J. Phys. Oceanogr.,* **11,** 324–336.

Lentz, S. J., 2001: The influence of stratification on the wind-driven cross-shelf circulation over the North Carolina shelf. *J. Phys. Oceanogr.,* **31,** 2749–2760.

——, 2004: The response of buoyant coastal plumes to upwelling-favorable winds. *J. Phys. Oceanogr.,* **34,** 2458–2469.

——, and K. R. Helfrich, 2002: Buoyant gravity currents along a sloping bottom in a rotating frame. *J. Fluid Mech.,* **464,** 251–278.

——, R. T. Guza, S. Elgar, F. Feddersen, and T. H. C. Herbers, 1999: Momentum balances on the North Carolina inner shelf. *J. Geophys. Res.,* **104,** 18 205–18 226.

——, K. Shearman, S. Anderson, A. Plueddemann, and J. Edson, 2003: Evolution of stratification over the New England shelf

during the Coastal Mixing and Optics study, August 1996–June 1997. *J. Geophys. Res.,* **108,** 3008, doi:10.1029/2001JC001121.

Munchow, A., and R. W. Garvine, 1993: Buoyancy and wind forcing of a coastal current. *J. Mar. Res.,* **51,** 293–322.

Pichevin, T., and D. Nof, 1997: The momentum imbalance paradox. *Tellus,* **49A,** 298–319.

Rennie, S., J. L. Largier, and S. J. Lentz, 1999: Observations of low-salinity coastal current pulses downstream of Chesapeake Bay. *J. Geophys. Res.,* **104,** 18 227–18 240.

Sanders, T. M., and R. W. Garvine, 2001: Fresh water delivery to the continental shelf and subsequent mixing: An observational study. *J. Geophys. Res.,* **106,** 27 087–27 101.

Simpson, J. E., 1982: Gravity currents in the laboratory, atmosphere, and ocean. *Annu. Rev. Fluid Mech.,* **14,** 213–234.

Stern, M. E., J. A. Whitehead, and B. L. Hua, 1982: The intrusion of the head of a gravity current along the coast of a rotating fluid. *J. Fluid Mech.,* **123,** 237–266.

Valle-Levinson, A., K.-C. Wong, and K. T. Bosley, 2001: Observations of the wind-induced exchange at the entrance to Chesapeake Bay. *J. Mar. Res.,* **59,** 391–416.

Whitney, M. M., and R. W. Garvine, 2005: Wind influence on a coastal buoyant outflow. *J. Geophys. Res.,* **110,** C03014, doi:10.1029/2003JC002261.

Xing, J., and A. M. Davies, 1999: The effect of wind direction and mixing upon the spreading of a buoyant plume in a non-tidal regime. *Cont. Shelf Res.,* **19,** 1437–1483.

Yankovsky, A. E., and D. C. Chapman, 1997: A simple theory for the fate of buoyant coastal discharges. *J. Phys. Oceanogr.,* **27,** 1386–1401.